



Review

Revisited Catalytic Hydrogen Evolution Reaction Mechanism of MoS₂

Yuhao He, Xiangpeng Chen, Yunchao Lei, Yongqi Liu and Longlu Wang *

College of Electronic and Optical Engineering & College of Flexible Electronics (Future Technology), Nanjing University of Posts and Telecommunications, Nanjing 210023, China; b20080216@njupt.edu.cn (Y.H.); 1221025306@njupt.edu.cn (X.C.); 1221025307@njupt.edu.cn (Y.L.); 1222025412@njupt.edu.cn (Y.L.)

* Correspondence: wanglonglu@njupt.edu.cn

Abstract: MoS₂ has long been considered a promising catalyst for hydrogen production. At present, there are many strategies to further improve its catalytic performance, such as edge engineering, defect engineering, phase engineering, and so on. However, at present, there is still a great deal of controversy about the mechanism of MoS₂ catalytic hydrogen production. For example, it is generally believed that the base plane of MoS₂ is inert; however, it has been reported that the inert base plane can undergo a transient phase transition in the catalytic process to play the catalytic role, which is contrary to the common understanding that the catalytic activity only occurs at the edge. Therefore, it is necessary to further understand the mechanism of MoS₂ catalytic hydrogen production. In this article, we summarized the latest research progress on the catalytic hydrogen production of MoS₂, which is of great significance for revisiting the mechanism of MoS₂ catalytic hydrogen production.

Keywords: catalytic mechanism; edge engineering; defect engineering; phase engineering

1. Introduction

Hydrogen energy is the ultimate environment-friendly energy and the most promising form of energy to replace traditional energy sources such as coal, oil, and natural gas [1–5]. At present, the production of hydrogen mainly relies on the cracking of traditional energy sources, which belongs to false decarbonization [6–8]. Hydrogen production by solar photovoltaic power generation is the most promising method of hydrogen production [9,10]. The key to electrocatalytic hydrogen production lies in the development and utilization of an electrocatalyst. Because the precious metal platinum has good catalytic hydrogen production performance, it is the best hydrogen production catalyst at present; however, its high cost and scarce resources seriously hinder its application in catalytic production.

As a non-precious metal catalyst with the most potential to replace precious metal platinum, MoS₂ has attracted increasing attention [11–16]. The key factors that determine the catalytic hydrogen production performance of MoS₂ mainly relate to two aspects: one is the number of active sites, and the other is the true activity of the active site [17–22]. It is generally believed that the base surface of MoS₂ is chemically inert and does not have the performance of catalytic hydrogen production; moreover, at the same time, the edge of MoS₂ has high catalytic hydrogen evolution activity [23–27]. More and more people are using various methods to expose the edge of MoS₂ to improve its catalytic hydrogen production performance [28–32]. The latest research shows that the conversion of sheet MoS₂ into bands can expose the edge sites and improve the catalytic hydrogen production performance [33–41]. It is also possible to directly generate branchlike MoS₂ by controlling the proportion of precursors during the growth of MoS₂, thereby increasing the edge site of MoS₂ [42–48]. Defect engineering and phase engineering are also strategies to regulate the catalytic hydrogen production performance of MoS₂ [49–56]. Although the catalytic hydrogen production performance of MoS₂ can be adjusted through various regulatory strategies, the corresponding catalytic mechanism is still very controversial. It has been



Citation: He, Y.; Chen, X.; Lei, Y.; Liu, Y.; Wang, L. Revisited Catalytic Hydrogen Evolution Reaction Mechanism of MoS₂. *Nanomaterials* **2023**, *13*, 2522. <https://doi.org/10.3390/nano13182522>

Academic Editor: Diego Cazorla-Amorós

Received: 16 August 2023

Revised: 30 August 2023

Accepted: 2 September 2023

Published: 8 September 2023



Copyright: © 2023 by the authors. Licensee MDPI, Basel, Switzerland. This article is an open access article distributed under the terms and conditions of the Creative Commons Attribution (CC BY) license (<https://creativecommons.org/licenses/by/4.0/>).

reported that the inert base plane can undergo a transient phase transition in the catalytic process to play the catalytic role, which is contrary to the common understanding that the catalytic activity only occurs at the edge [57].

Only a deep and correct understanding of the catalytic mechanism of MoS₂ can further promote the design of high-performance MoS₂ structures, so as to promote the improvement of its catalytic performance. With the help of first principles theoretical calculation and in situ characterization, the catalytic process can be understood from the molecular and atomic levels and the mechanism of catalytic hydrogen production can be revealed. In this review, we introduce the latest research progress of strategies to improve the performance of MoS₂ catalytic hydrogen production and give prospects for the development and direction of this research field.

2. Edge

It is well known that the edge site of MoS₂ has high catalytic HER activity, and a lot of research has focused on how to expose the edge of MoS₂. Recent studies have shown that the MoS₂ can be designed with a rich edge structure such as a paired edge nanoribbon, which can further enhance the catalytic HER activity of MoS₂.

2.1. Nanoribbon

According to research on edge-dominated electrochemical reaction kinetics in ultra-narrow MoS₂ nanoribbons, ideal energetics for HER could be obtained. Large arrays of MoS₂ nanoribbons were acquired using a templated subtractive patterning process (TSPP), which significantly enhanced the turn-over frequency, exchanged the current density, and lowered the Tafel slope because of improved charge transfer efficiency.

Utilizing the naturally occurring bilayer and multilayer regions in graphene, and taking advantage of the bottom-up approach of graphene, the pattern is transferred from the graphene mask to the surface of the MoS₂ material through a pattern transfer process, thus forming an aligned MoS₂ nanoribbon array with a controlled direction, as shown in Figure 1a. Since the formation of nanoribbons is random to a certain extent, the width distribution is also affected in Figure 1b. With a length-to-width ratio of more than 7000 and a high density (Figure 1c), the strips are more efficient than other strategies for patterning MoS₂ nanoribbons. The observation of a single nanoribbon over a long distance in Figure 1d shows that the fractures are solved and the structural stability of the nanoribbon is ensured. Using the electron diffraction technique, the crystal properties of MoS₂ nanoribbons can be determined and characterized. The six-fold symmetry diffraction pattern in Figure 1e was observed using the SAED model. Through an analysis of the multiple SAED patterns presented in Figure 1f, the orientation of the nanoribbon was determined not to affect the crystal structure. The atomic arrangement in the TEM in Figure 1g shows an orderly structure with no obvious defects. The difference in brightness may be due to the atomic number of the atoms; the darker atoms are Mo and the brighter ones are of S. High basal plane quality, which makes their nanoribbon array an ideal model system for studying the source of HER enhancement. A three-electrode localized electrochemical microcell technique was employed to conduct electrochemical research. Consisting of an exposed reaction window and gold contact, as shown in the schematic of the microelectrode structure in Figure 1h,i, it may be used to place droplets for electrochemical studies. As shown in Figure 1j, the HER exchange current of the MoS₂ nanoribbon arrays is significantly larger than that of pristine flakes, and the overpotential shows a decrease of 41%, which reveals an improved HER thermodynamic performance. Because the device is not deposited on a conductive surface and the carrier passes laterally through the nanoribbons from the electrode, introducing an uncompensated resistance, HER kinetics is quantified with the fitted Tafel curve. The Tafel slope of the pristine flake is consistent with previous results. As a comparison, the nanoribbon arrays' Tafel slope in Figure 1k greatly decreased, showing the impact of edges on the improved HER kinetics of MoS₂. It can also be pointed out that

the observed Tafel slope is in good agreement with prior findings on edge-enriched, 2D materials, and it exhibits a clear distinction from alternative functionalization approaches.

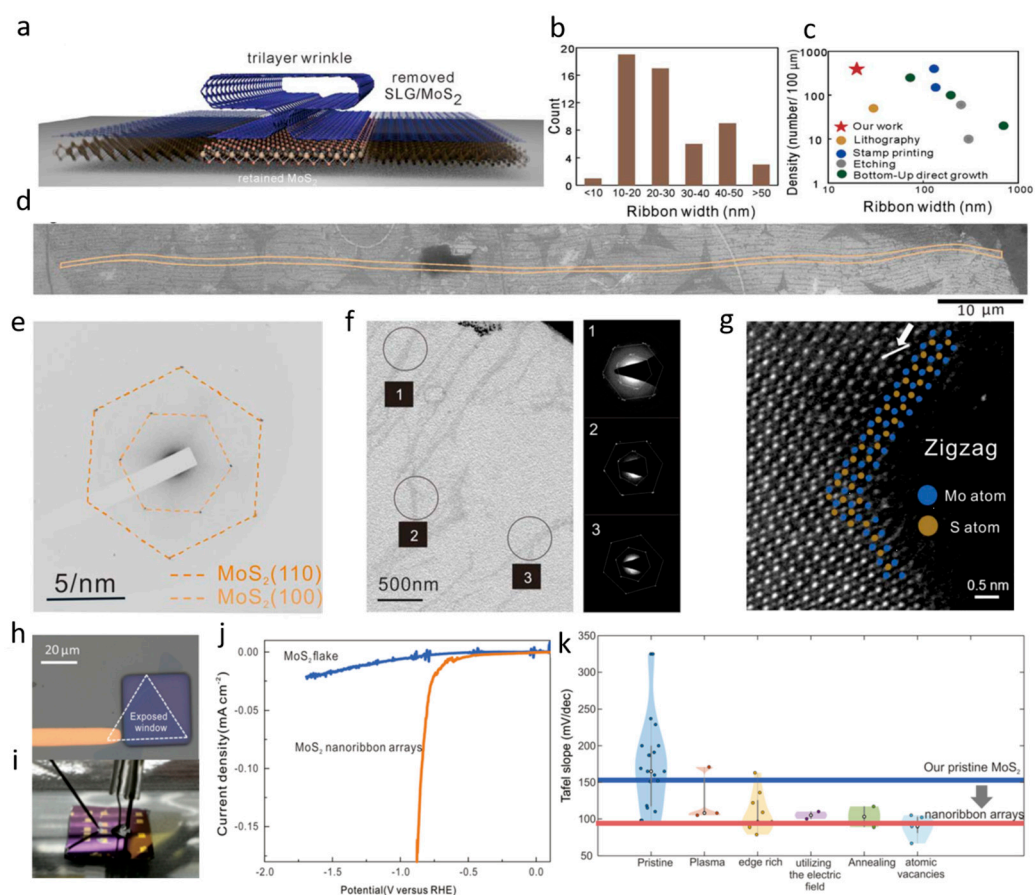


Figure 1. (a) Schematic representation of the wrinkle-templated nanoribbon formation. (b) A histogram that depicts the width distribution of nanoribbons was determined through an analysis of transmission electron images. (c) A comparison between the attainable width and array density of nanoribbons in this study and previous results. (d) Composite SEM image with a nanoribbon exceeding 100 μm . (e) A selected area diffraction pattern that indicates the symmetry of MoS_2 . (f) A low-resolution TEM image with SAED patterns, demonstrating that three distinct areas exhibit long-range atomic alignment. (g) An atomic resolution TEM image reveals the orientation of the lattice structure. (h) An optical micrograph displays a monolayer of 2H- MoS_2 , showing an exposed reaction window and a gold contact. (i) A photograph illustrating the capillary microcell employed for HER measurements. (j) Comparison between the performance of a MoS_2 flake and a nanoribbon array using polarization curves. (k) A comparative analysis between literature values of pristine and modified 2H- MoS_2 and the results obtained in this study. Adapted with permission from [53], Copyright 2023 Royal Society of Chemistry.

2.2. Fractal MoS_2

Since the catalytic active site of 2H- MoS_2 is mainly at its edge, controlling the morphology and structure of MoS_2 to expose more edges can further improve the hydrogen evolution reaction (HER) of MoS_2 . Then, if MoS_2 is grown in a multi-branched and multi-edge morphology structure in the chemical vapor deposition (CVD) growth process, the HER performance of MoS_2 can be improved. Therefore, Yu G. et al. synthesized MoS_2 with different morphologies by adjusting the proportion of precursor in the process of MoS_2 generation by CVD.

As shown in Figure 2a,b, fractal MoS_2 and triangular MoS_2 were obtained by controlling the proportions of MoO_3 and S, respectively, and the coverage rate of fractal MoS_2

and triangular MoS₂ was determined to be 20.5% and 22.7% using image analysis software. When MoO₃ is sufficient, a triangular MoS₂ can be generated, while, at a low dose of MoO₃, a fractal MoS₂ will be generated. After the formation of MoS₂ with different morphologies, their catalytic properties were further evaluated. Figure 2c shows the polarization curves of the two MoS₂ samples, the GC electrode and Pt foil. Compared with triangular MoS₂, fractal MoS₂ has a smaller initial hydrogen evolution overpotential; moreover, as shown in Figure 2d, the Tafel slope of the fractal MoS₂ is lower than that of the triangular MoS₂. It is therefore confirmed that the fractal MoS₂ has more active edges and better catalytic activity.

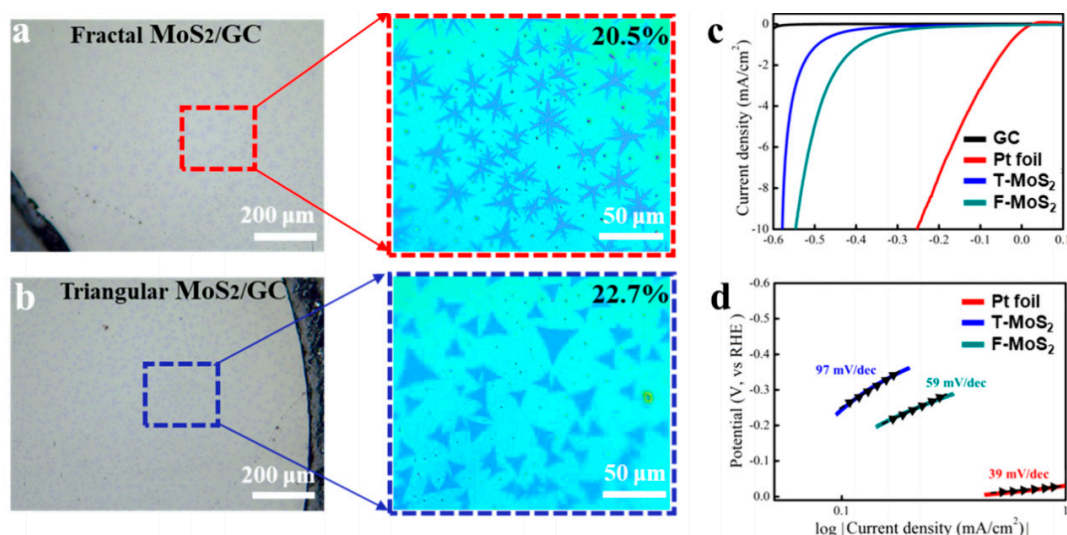


Figure 2. (a,b) Optic microscopy (OM) images of different kinds of MoS₂ transferred to the glassy carbon (GC) electrode, (c) polarization curves of the two MoS₂ samples, and (d) the Tafel slope diagram. Adapted with permission from [54], Copyright 2022 American Chemical Society.

3. Sulfur Vacancies

Vacancies are considered to be the limiting doping states that promote atomic rearrangements and modulate the electronic structure over a wide range. Many methods have been successfully implemented to introduce vacancies in 2D TMDs, such as hydrogen plasma exposure, H₂ annealing, Ar²⁺ beam irradiation, and helium ion beam irradiation, showing great potential for catalytic reactions. However, all of the above methods require additional intervention from external stimuli; therefore, it is difficult to generate controllable vacancies directly by growth.

Defect engineering is an effective strategy to accelerate the catalytic hydrogen production performance of MoS₂. However, introducing defects such as sulfur vacancies on the MoS₂ basal plane is still a major challenge. Currently, sulfur vacancies are mainly introduced into MoS₂ by using post-treatment methods such as plasma treatment, ultrasonic, ball milling, and other methods. However, if sulfur vacancies can be introduced directly during the preparation of MoS₂, it would be an excellent strategy to prepare sulfur vacancy defects.

As shown in Figure 3a, Man et al. proposed that sulfur vacancies can be introduced into the MoS₂ basal plane by controlling the reaction conditions during the MoS₂ growth through a salt-assisted CVD method [55]. The density of sulfur vacancies could be controllable by controlling the added amount of KCl during the CVD growth process, and some kind of change has occurred during the process. Figure 3b shows the luminescence spectra of the obtained MoS₂ with different densities of sulfur vacancies, and it was found that the luminescence intensities of the obtained samples were different when the added amount of KCl was different, which indicates that the density of sulfur vacancies is positively correlated with the added amount of KCl. It is noted that the energy band holds steady when the added KCl reaches a certain amount. The density of sulfur vacancies could

be successfully controlled using this salt-assisted CVD method. In order to explore the relationship between the density of sulfur vacancies and the catalytic hydrogen production performance of MoS₂, a micro-nano HER test platform was built (shown in Figure 3c,d) to precisely evaluate the catalytic performance of monolithic MoS₂ with sulfur vacancies. It was found that the samples with abundant sulfur vacancies had the best catalytic hydrogen production performance and the lowest Tafel slope (Figure 3e,f). The overpotential was negatively correlated with the concentration of added KCl (Figure 1g), which confirmed that the sulfur vacancies of MoS₂ could be active sites for catalytic hydrogen production. The catalytic hydrogen production performance becomes much better when the density of sulfur vacancies is higher. Figure 1h shows the relationship between the overpotential and Tafel slope of all the samples along with sulfur vacancy as reported in other literature. It could be seen that the sample obtained by this work has the best catalytic performance, which indicates that the salt-assisted CVD method is an excellent strategy for creating the sulfur vacancies that serve as HER catalytic active sites.

The method of thermochemical annealing sodium hypophosphite to produce MoS₂-active defects is proposed; meanwhile, it can spontaneously produce PH₃ to regulate the MoS₂ lattice. By controlling the reaction conditions, active defects are formed at the basal plane and edges, thereby exposing more metal active sites and improving the Hydrogen Evolution Reaction (HER) performance of MoS₂. The development of efficient and low-cost MoS₂ catalysts for practical applications is important. Sodium hypophosphate is set at around 200 °C to produce PH₃ gas, and MoS₂ is annealed using PH₃ gas at 500 °C as shown in Figure 4a. PH₃ reacts with MoS₂ to produce defects that replace the S atom in the MoS₂ lattice through defects, resulting in P doping (Figure 4b). Due to the active chemical properties of doped P, the active P element can be oxidized to a phosphate layer coating on the surface of MoS₂ and form phosphate without phosphate compounds in the MoS₂ crystal. The phosphate could be eventually removed from the crystal lattice of the MoS₂ crystal if it is dissolved in water or acid solution, thus creating defects again. Active defects may provide additional adsorption sites or change the local environment of the atom. When the proton is adsorbed to active defects from a relatively stable state, the ΔG_{H^*} (Gibbs free energy) of the system will change to regulate the thermodynamic adsorption/desorption of the proton. Energy level inhomogeneity can also be introduced to regulate the interface energy level and facilitate electron transport, which ultimately optimizes HER activity (Figure 4c). To further explore the more important factors affecting HER activity, a microelectrochemical reactor was used to distinguish the influence of interfacial charge injection and thermodynamic adsorption. As shown in the schematic, this is the cross-section of monolayer graphene and a PH₃-treated monolayer MoS₂ electrochemical device (Figure 4d). The performance of a single MoS₂, rather than the whole catalyst, can be directly investigated in a microelectrochemical reactor, and the enhanced HER activity due to specific factors can be demonstrated. Graphene and unannealed/annealed MoS₂ monolayer nanosheets were prepared as contact electrodes and target catalysts, respectively. Comparing the relative overpotential of the four devices, it was found that the overpotential of the graphene-pMoS₂ heterostructure device was -100 mV at $10 \text{ mA}\cdot\text{cm}^{-2}$, which was much smaller than that of the other three devices, and the Tafel slope gradually decreased from curve 4 to 1 (Figure 4e). The difference of curves in overpotential caused by charge transfer for 3 to 4 is -32 mV, while 1 to 2 is -60 mV. The thermodynamic ΔG_{H^*} is -140 mV for 1 to 3 and -112 mV for 2 to 4. It can be concluded from the data that charge transfer plays a less important role than thermodynamic ΔG_{H^*} due to drastic changes in properties.

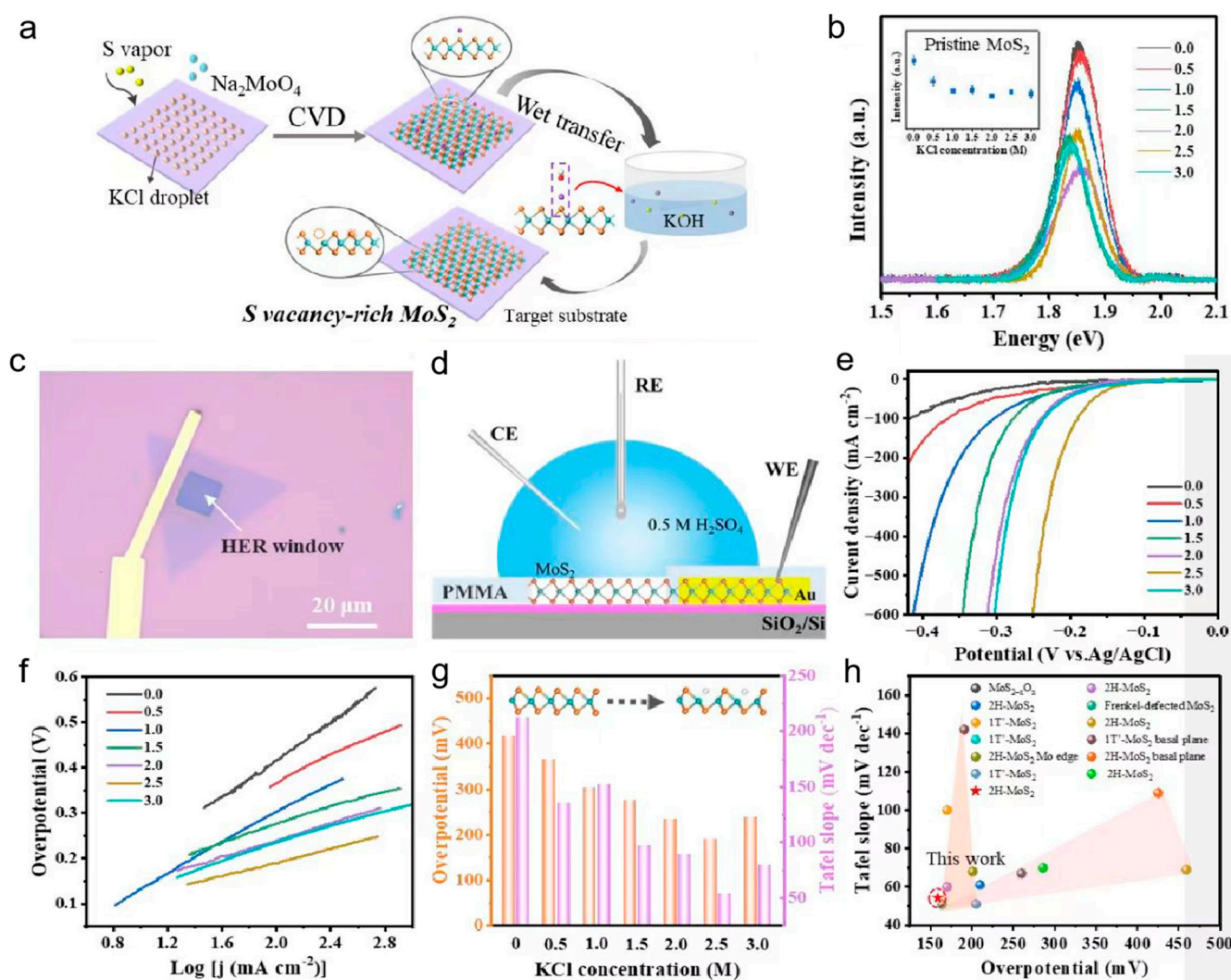


Figure 3. (a) Schematic illustration of the CVD growth of vacancy-rich MoS₂. (b) Spectra of MoS₂ basal plane under various KCl concentrations from 0.0 to 3.0 M. The inset shows the statistical results of PL intensity under each concentration (C_{KCl}). (c) Optical image and (d) schematic of the as-fabricated MoS₂ microdevice. WE: work electrode, RE: reference electrode, CE: counter electrode. (e) LSV curves and corresponding (f) Tafel plots of the MoS₂-KCl microdevices. (g) Comparison of overpotentials (red) and Tafel slopes (orange) under different KCl concentrations. (h) A comparison between the Tafel slope and overpotential of this work and the reported MoS₂-based catalysts. Adapted with permission from [55], Copyright 2023 Wiley-VCH GmbH.

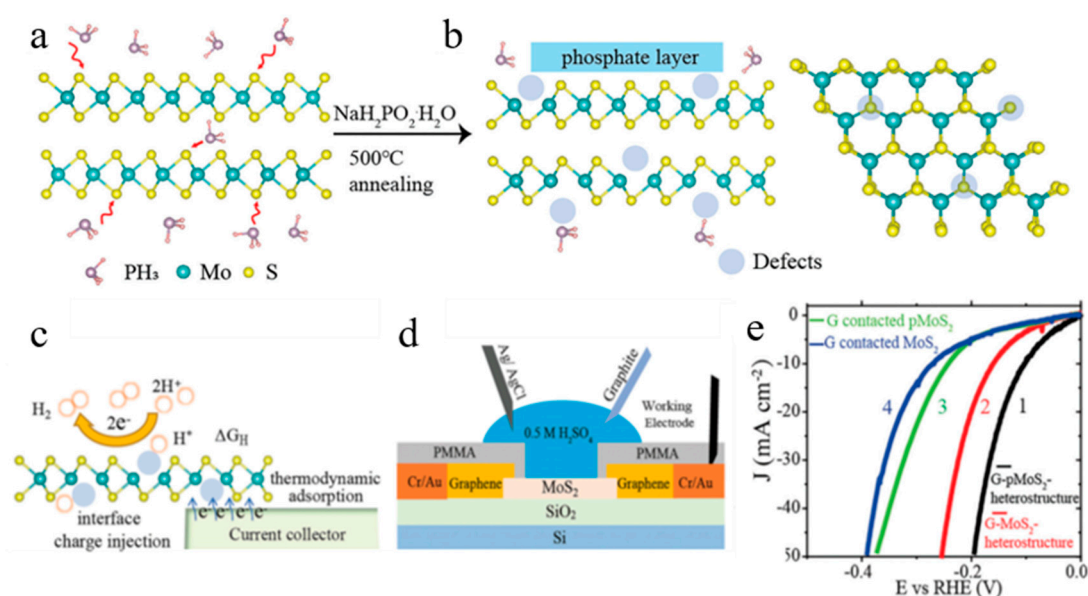


Figure 4. (a) Schematic of PH₃ molecule extracting sulfur atoms from the MoS₂ layers. (b) The defects' formation in the basal planes, point/line defects, and edges, resulting in H₃PO₄ layers on top of MoS₂ catalysts. (c) Schematic comparison of thermodynamic hydrogen adsorption and interface charge injection that determined the performance of hydrogen evolution reaction. (d) Schematic cross-section view of monolayer graphene and PH₃-treated monolayer MoS₂ electrochemical device. (e) Normalized polarization curves measured from different graphene and MoS₂ devices. Adapted with permission from [56], Copyright 2023 Wiley-VCH GmbH.

4. Doping

Doping engineering has become an effective strategy to improve MoS₂ base activity [57]. The most common doping engineering practice is to improve its electronic structure through heteroatom doping, thereby enhancing its intrinsic catalytic activity. This is mainly because the electronic structure of the base atoms is modulated using defect engineering to improve its surface conductivity [58]. In addition, heteroatom doping has important effects on chemical bond formation, adsorption/desorption processes, and the Gibbs free energy of the reaction [59–62]. Therefore, the electrocatalytic activity of MoS₂-based catalysts can be effectively improved according to the electronegativity difference and the type and number of heteroatoms.

1T-phase MoS₂ (1T-MoS₂) has been widely concerned in hydrogen evolution reaction (HER) because it exhibits better charge transport characteristics and can expose more active sites. Although 1T-MoS₂ is a good HER material under acidic conditions, it produces a higher overpotential under alkaline conditions. At the same time, the conditions of an alkaline solution are more suitable for HER.

The design and modification of the catalytic site at the atomic level can deepen the understanding of the active site of the catalyst, which is essential to enhance the activity of the catalyst. In this regard, Jing Gu et al. used Anderson-type polyoxometalates as a precursor to doping the metal active site onto 1T-MoS₂ at the atomic level to improve the HER activity of 1T-MoS₂. As shown in Figure 5a,b, the precursor Anderson-type POM nanoclusters, [XH₆Mo₆O₂₄]ⁿ⁻ (denoted as XMo₆, where X represents the doped metal atoms such as Fe, Co, Ni, etc.) is characterized by different shapes. Figure 1c shows the resultant XO@1T-MoS₂ structure. Figure 5d shows the synthesis process using XMo₆ to construct XO@1T-MoS₂ on highly conductive carbon fiber paper (CFP) by vulcanizing the hydrothermal reaction. It is generally considered that ΔG (H₂O) ΔG (H^{*}) is important for understanding HER catalytic activity in the alkaline medium HER process. Using the density functional theory (DFT) calculation, the structure of XO@1T-MoS₂ and the free energy diagram of the catalyst surface during the reaction were constructed. As shown in

Figure 5e, the structure of $XO@1T-MoS_2$ consists of a hexagonal XMo_6S_{14} unit with six Mo atoms surrounding the X atom. As shown in Figure 5f, the calculated Gibbs free energy shows that the $\Delta G(H^*)$ of $1T-MoS_2$ doped with transition metal is significantly reduced. The $\Delta G(H^*)$ of $Ni@1T-MoS_2$ is close to 0, indicating that it can promote the desorption of H^* . At the same time, the addition of transition metals also significantly reduces $\Delta G(H_2O)$ and promotes the dissociation of H_2O to H^* . Then, the synergistic effect of oxygen and Ni was studied by controlling the amount of oxygen incorporation. It was found that $\Delta G(H_2O)$ and $\Delta G(H^*)$ were further reduced with the addition of oxygen, while excess oxygen would increase them. In summary, the HER properties of the catalyst can be promoted by incorporating transition metal and appropriate oxygen into $1T-MoS_2$.

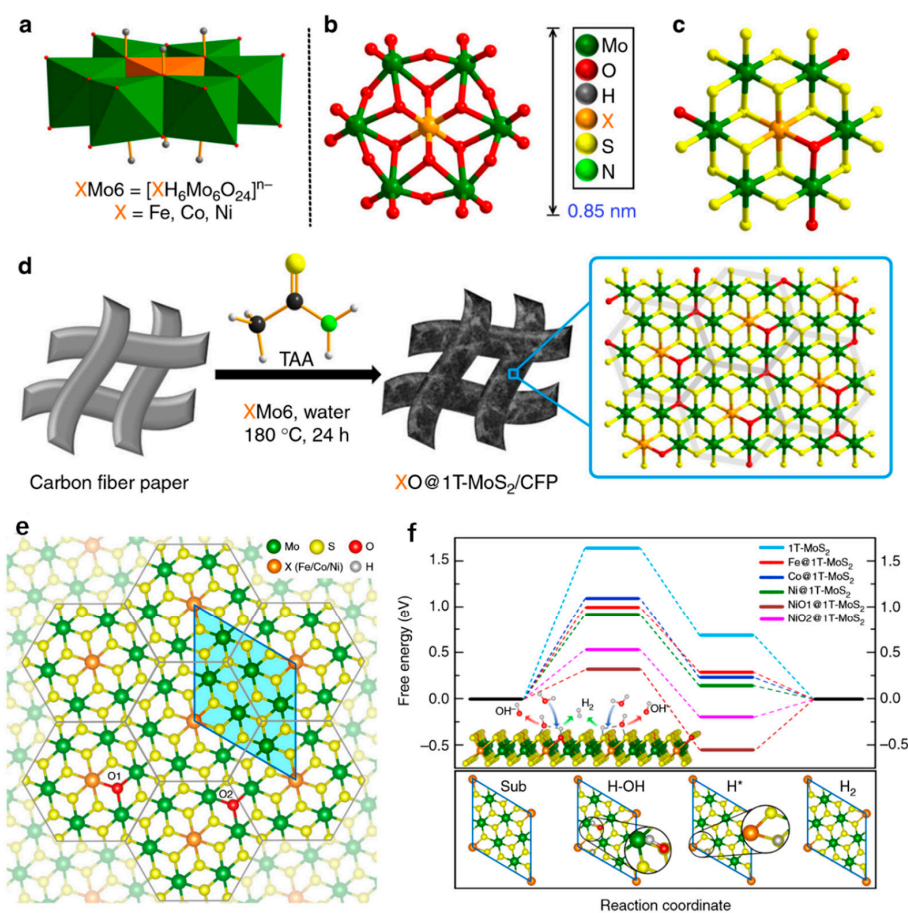


Figure 5. (a) Polyhedral characterization of XMo_6 precursors. (b) Spherical and rod-like characterization of XMo_6 precursors. (c) Mode structure of $XO@1T-MoS_2$. (d) Diagram of the preparation of atomic scale transition metal and oxygen co-doped $1T-MoS_2$ nanosheets on carbon fiber paper (CFP) using incomplete vulcanization of XMo_6 . (e) Single-layer structure of $X@1T-MoS_2$ formed by O co-doped XMo_6 hexagonal primitive. (f) Surface free energy diagram of different catalysts in alkaline solution. Adapted with permission from [63], Copyright 2019 Nature Publishing Group.

5. Phase

It is generally believed that the base plane of MoS_2 is inert; however, it has been reported that the inert base plane can undergo a transient phase transition in the catalytic process to play the catalytic role, which is contrary to the common understanding that the catalytic activity is only at the edge. The HER catalytic mechanism of $1T-MoS_2$ remains elusive and controversial. Therefore, it is necessary to further understand the mechanism of MoS_2 catalytic hydrogen production.

5.1. An Irreversible Phase Transition during Photocatalytic Hydrogen Evolution

It is widely believed the active sites of 2H-MoS₂ for catalytic hydrogen production are located at the edges, while its basal plane is inert. Moreover, it has been reported that the conversion of the 2H phase into the 1T phase by phase transformation is an ideal strategy to enhance the catalytic HER performance of MoS₂. However, the HER catalytic mechanism of 1T-MoS₂ remains elusive and controversial. It is difficult to explain the nature of the better catalytic performance, which is originally from the improved electrical conductivity, the increased intrinsic activity of the active site, or the number of active sites.

In order to explore this problem, the Wang group made ultra-thin MoS₂ nanosheets that were vertically grown on TiO₂ nanofibers, and this vertical growth could introduce the strain. The 1T-MoS₂ with sulfur vacancies and strain could be obtained by further lithium intercalation. As shown in Figure 6a, using this sample as the catalyst for HER, it was found that its catalytic performance gradually increased during the process of catalytic hydrogen production. It was also found that the catalytic hydrogen production per hour increased gradually with time in Figure 6b. This self-optimization of the catalytic performance is most likely due to the structural transformation of the catalyst during the catalytic HER process. In order to investigate this transformation, the catalyst after the catalytic reaction was structurally traced. The HRTEM in Figure 6c,d shows that the 1T phase has transformed into the 1T' phase, with the super-lattice structure from the Mo atom clustering into Zigzag chains. This suggests that the 1T' phase is the true active phase for catalytic HER. A molecular dynamics simulation was performed to research the transition from the 1T phase to the 1T' phase (Figure 6e). It was found that the 1T phase with surface-adsorbed hydrogen was more easily converted to the 1T' phase, which means that the surface-adsorbed hydrogen could promote the transformation of the 1T phase to the 1T' phase. This is sufficient to show that, in the photocatalytic HER process, the 1T phase with adsorbed hydrogen atoms on the surface could transform into the 1T' phase with high activity, which leads to the phenomenon of the self-optimization of the catalytic performance. This work therefore reveals the catalytic mechanism of 1T-phase MoS₂.

5.2. Transient Phase Transition during the Hydrogen Evolution Reaction

2H-MoS₂ is one of the most promising noble metal-free electrocatalysts in the hydrogen evolution reaction (HER). With regard to its HER mechanism, the widely accepted view, so far, is that its marginal sites have high HER activity, while its basal plane is inert during the HER process. However, Zhai et al. found that this conclusion was incorrect and verified it using ATR-SEIRAS and XAFS. The three-electrode ATR-SEIRAS cell used for the in situ measurement is shown in Figure 7a. As shown in Figure 7b, 0.5M H₂SO₄ was added to the three-electrode ATR-SEIRAS cell as the electrolyte, and the ATR-SEIRAS spectra of MoS₂ at −0.1 V, −0.2 V, −0.3 V and after reaction were measured. It can be found that a peak of 2523 cm^{−1} occurs at −0.2 V and −0.3 V, and this peak is not from the edge site; rather, a continuous peak of 2600 cm^{−1} is from the edge site. The formation of the S–H bond was observed at −0.2 V, indicating that 2523 cm^{−1} in the experiment is the stretching vibration of the S–H bond ($\nu(\text{S-H})$). Then, as shown in Figure 7c, the stretching vibration of the S–H bond is calculated and compared with the experimental value. There are two adsorption modes of the S–H bond in 2H-MoS₂, namely, vertical adsorption and inclined adsorption. However, the calculated values of the $\nu(\text{S-H})$ of the two models differ greatly from the experimental results. Similarly, the S–H bond in 1T'-MoS₂ also has two adsorption modes, which are, respectively, in the higher position and the lower position and are denoted as S-H and S-L. It is found that $\nu(\text{S-H})$ on S-L has a good agreement with the experimental value. In addition, as shown in Figure 1d,e, when the electrolyte H₂SO₄ in the experiment was replaced by D₂SO₄, that is, when the proton source in the HER process was replaced by D, the conclusion remained unchanged, and $\nu(\text{S-H})$ on S-L also had a good agreement with the experimental value. The experimental results show that there is a phase transition from 2H to 1T' during the reaction. As shown in Figure 7f–k, in order to further verify that the 2H to 1T' phase transition is not permanent but transient, the EXAFS diagram during

the reaction process and the wavelet transform analysis of 2H-MoS₂ were measured. As shown in Figure 7f, under open-circuit potential (OCP), the length of the Mo–S bond and Mo–Mo bond is consistent with those of 2H-MoS₂, while the length of the Mo–Mo bond is consistent with 1T'-MoS₂ at –0.2 V and –0.3 V. It is found that the characteristics of 1T'-MoS₂ disappear after the end of the reaction, indicating that this phase transition is transient. As shown in Figure 7g–k, the WT data further indicate that this phase transition is transient, and no 1T'-MoS₂ feature appears at OCP and –0.1 V, and the 1T'-MoS₂ feature appears at –0.2 V; moreover, this feature is more obvious at –0.3 V, and, when the reaction ends, the feature of 1T'-MoS₂ disappears. In conclusion, Zhai et al. verified that part of the base phase of 2H-MoS₂ would change into 1T'-MoS₂ during the HER process, showing high activity, and that 1T'-MoS₂ would change into 2H-MoS₂ after the reaction.

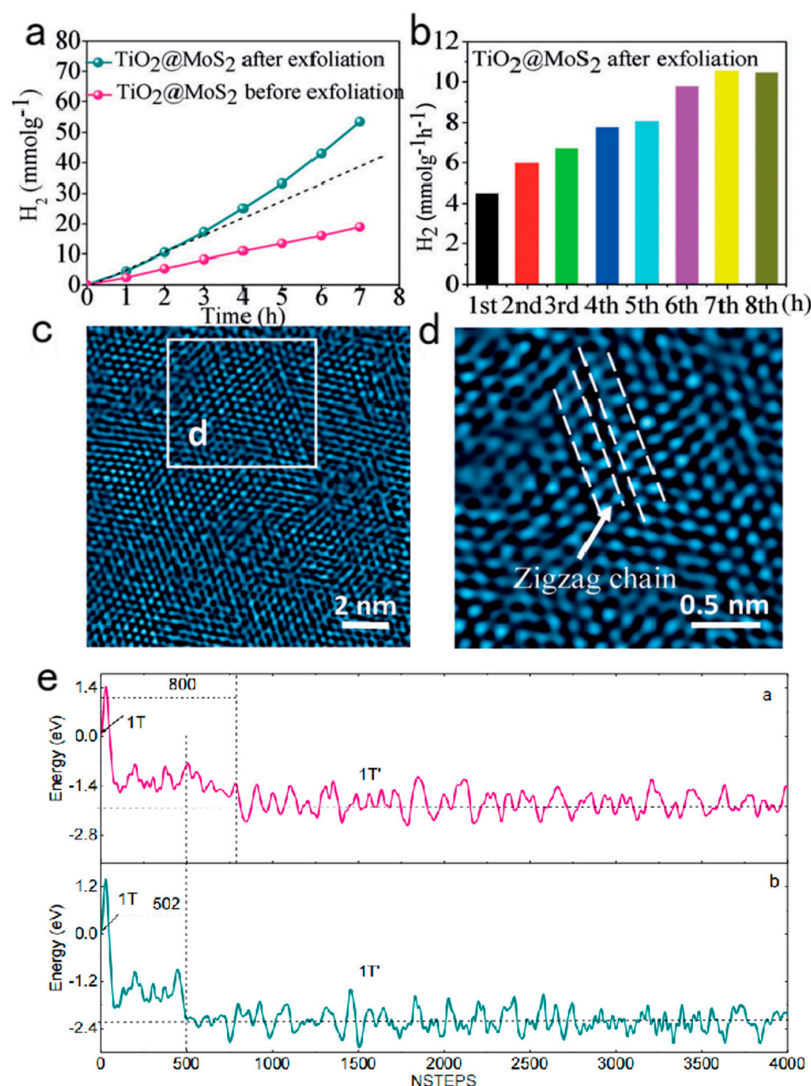


Figure 6. (a) H₂ accumulation and (b) H₂ production rate over exfoliated TiO₂@MoS₂ at each hour of the HER. All experiments were carried out in 80 mL of 15% (v/v) TEOA aqueous solution under visible light irradiation ($\lambda > 420$ nm). Catalysts: 20 mg and EY: 20 mg. (c) HRTEM image of the MoS₂ in the exfoliated TiO₂@MoS₂ after 7 h HER. (d) Enlarged view of the square in c (the arrow points to the zigzag chain configuration of 1T'). (e) Evolution of total electronic energy using AIMD simulations in the MoS₂ phase transformation at 298 K. (a—1T phase MoS₂ transform into 1T' phase spontaneously; b—1T phase MoS₂ with 1/16 H coverage transform into 1T' phase). Adapted with permission from [13], Copyright 2017.

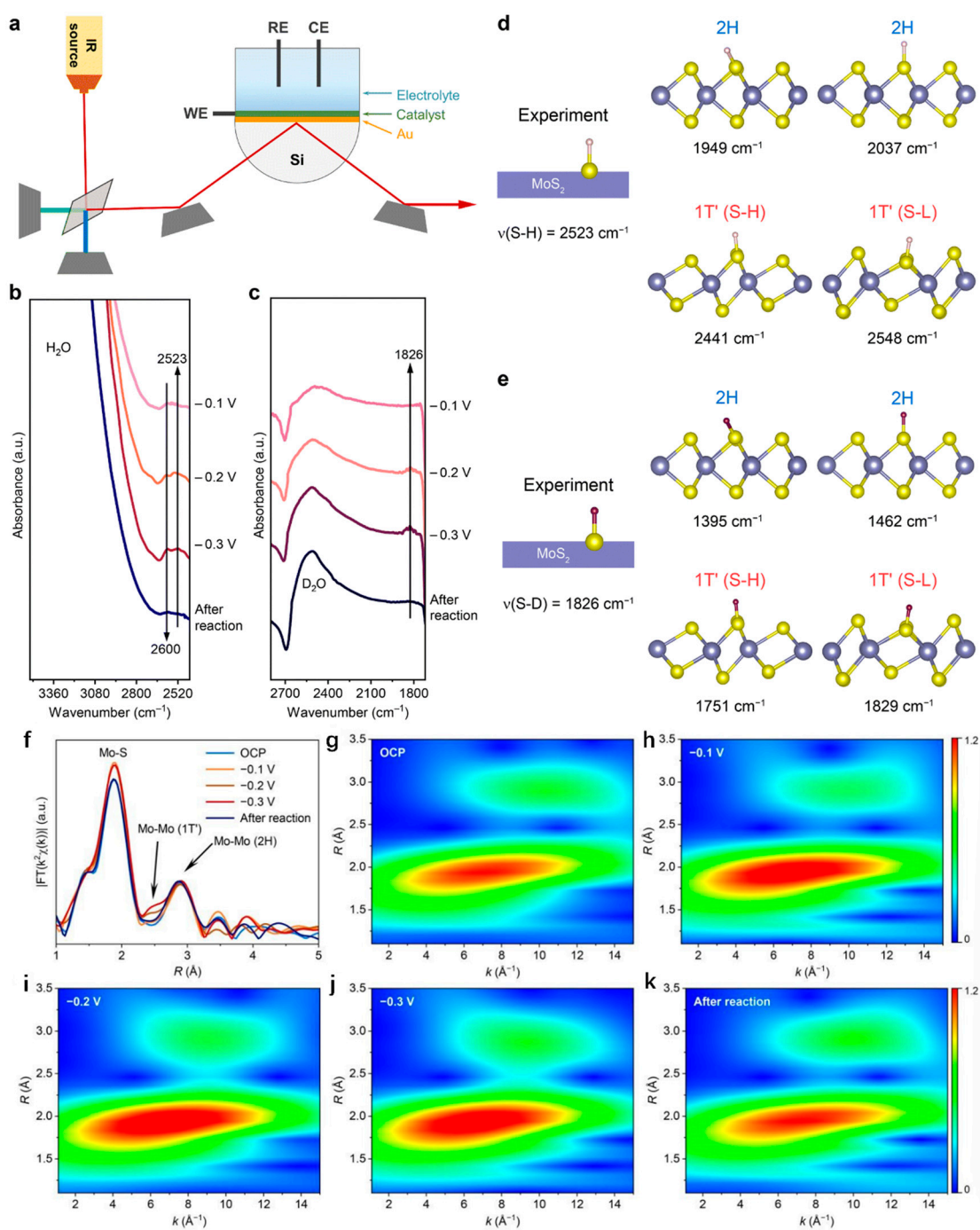


Figure 7. (a) Schematic diagram of a three-electrode ATR-SEIRAS cell measured in situ. (b) ATR-SEIRAS spectra of -0.1 V, -0.2 V, -0.3 V, and after the reaction measured in 0.5 M H_2SO_4 electrolyte and (c) 0.5 M D_2SO_4 electrolytes. (d) Comparison of $\nu(\text{S-H})$ experimental data and calculated data of 2H-MoS_2 and $1\text{T}'\text{-MoS}_2$. (e) Comparison of experimental and calculated data of $\nu(\text{S-D})$ of 2H-MoS_2 and $1\text{T}'\text{-MoS}_2$ after electrolyte replacement. The S atom is divided into S-H and S-L according to its position on $1\text{T}'\text{-MoS}_2$. (f) In situ EXAFS spectra of 2H-MoS_2 with respect to reversible hydrogen electrodes (RHEs) at OCP, -0.1 V, -0.2 V, and -0.3 V and after reaction. (g–k) Wavelet transform (WT) analysis of 2H-MoS_2 at (g) OCP, (h) at -0.1 V, (i) at -0.2 V, (j) at -0.3 V, and (k) after the reaction. Adapted with permission from [64], Copyright 2023 Royal Society of Chemistry.

6. Conclusions and Outlook

A number of strategies have been developed to improve the catalytic production performance of MoS₂, and the mechanism of MoS₂ catalytic hydrogen production has also been proposed. It is necessary to summarize and reconsider the latest mechanism of catalytic hydrogen production. In this review, we summarized the latest strategies to improve the catalytic hydrogen production of MoS₂ and the mechanism of catalytic performance improvement. We believe that, in this research field, it is necessary to further promote the improvement of MoS₂ catalytic hydrogen production performance from the following aspects. The catalyst with an ideal atomic structure should be prepared in view of the controversy over the mechanism of MoS₂ catalytic hydrogen production, and the catalyst should be used as a model to explore the mechanism of catalytic hydrogen production, combined with first-principles calculation and in situ characterization methods. The catalytic hydrogen production performance of MoS₂ should be standardized by constructing a micro-nano structure device, and the catalytic hydrogen production performance should be attributed to the catalytic active site with a specific atomic structure.

Funding: This work was financially supported by the Natural Science Foundation of China (51902101), the Youth Natural Science Foundation of Hunan Province (2021JJ540044), the Natural Science Foundation of Jiangsu Province (BK20201381), and the Science Foundation of Nanjing University of Posts and Telecommunications (NY219144).

Institutional Review Board Statement: Not applicable.

Informed Consent Statement: Not applicable.

Data Availability Statement: Not applicable.

Conflicts of Interest: The authors declare no conflict of interest.

References

1. Jaramillo, T.F.; Jørgensen, K.P.; Bonde, J.; Nielsen, J.H.; Horch, S.; Chorkendorff, I. Identification of active edge sites for electrochemical H₂ evolution from MoS₂ nanocatalysts. *Science* **2007**, *317*, 100–102. [[CrossRef](#)] [[PubMed](#)]
2. Voiry, D.; Yang, J.; Chhowalla, M. Recent strategies for improving the catalytic activity of 2D TMD nanosheets toward the hydrogen evolution reaction. *Adv. Mater.* **2016**, *28*, 6197–6206. [[CrossRef](#)] [[PubMed](#)]
3. Chang, C.; Wang, L.; Xie, L.; Zhao, W.; Liu, S.; Zhuang, Z.; Liu, S.; Li, J.; Liu, X.; Zhao, Q. Amorphous molybdenum sulfide and its Mo-S motifs: Structural characteristics, synthetic strategies, and comprehensive applications. *Nano Res.* **2022**, *15*, 8613–8635. [[CrossRef](#)]
4. Greeley, J.; Jaramillo, T.F.; Bonde, J.; Chorkendorff, I.; Nørskov, J.K. Computational high-throughput screening of electrocatalytic materials for hydrogen evolution. *Nat. Mater.* **2006**, *5*, 909–913. [[CrossRef](#)]
5. Voiry, D.; Fullon, R.; Yang, J.; de Carvalho Castro e Silva, C.; Kappera, R.; Bozkurt, I.; Kaplan, D.; Lagos, M.J.; Batson, P.E.; Gupta, G.; et al. The role of electronic coupling between substrate and 2D MoS₂ nanosheets in electrocatalytic production of hydrogen. *Nat. Mater.* **2016**, *15*, 1003–1009. [[CrossRef](#)]
6. Li, H.; Tsai, C.; Koh, A.L.; Cai, L.L.; Contryman, A.W.; Fragapane, A.H.; Zhao, J.H.; Han, H.S.; Manoharan, H.C.; Abild-Pedersen, F.; et al. Activating and optimizing MoS₂ basal planes for hydrogen evolution through the formation of strained sulphur vacancies. *Nat. Mater.* **2016**, *15*, 48–53. [[CrossRef](#)]
7. Lin, L.X.; Sherrell, P.; Liu, Y.Q.; Lei, W.; Zhang, S.W.; Zhang, H.J.; Wallace, G.G.; Chen, J. Engineered 2D transition metal dichalcogenides—A vision of viable hydrogen evolution reaction catalysis. *Adv. Energy Mater.* **2020**, *10*, 1903870. [[CrossRef](#)]
8. Sun, C.; Wang, L.; Zhao, W.; Xie, L.; Wang, J.; Li, J.; Li, B.; Liu, S.; Zhuang, Z.; Zhao, Q. Atomic-Level Design of Active Site on Two-Dimensional MoS₂ toward Efficient Hydrogen Evolution: Experiment, Theory, and Artificial Intelligence Modelling. *Adv. Funct. Mater.* **2022**, *32*, 2206163. [[CrossRef](#)]
9. Lu, Q.P.; Yu, Y.F.; Ma, Q.L.; Chen, B.; Zhang, H. 2D transition metal-dichalcogenide-nanosheet-based composites for photocatalytic and electrocatalytic hydrogen evolution reactions. *Adv. Mater.* **2016**, *28*, 1917–1933. [[CrossRef](#)]
10. He, Q.; Wang, L.; Yin, K.; Luo, S. Vertically aligned ultrathin 1T-WS₂ nanosheets enhanced the electrocatalytic hydrogen evolution. *Nanoscale Res. Lett.* **2018**, *13*, 167. [[CrossRef](#)]
11. Chen, J.; Tang, Y.; Wang, S.; Xie, L.; Chang, C.; Cheng, X.; Liu, M.; Wang, L.; Wang, L. Ingeniously designed Ni-Mo-S/ZnIn₂S₄ composite for multi-photocatalytic reaction systems. *Chin. Chem. Lett.* **2022**, *33*, 1468–1474. [[CrossRef](#)]
12. Wang, H.T.; Lu, Z.Y.; Kong, D.S.; Sun, J.; Hymel, T.M.; Cui, Y. Electrochemical tuning of MoS₂ nanoparticles on three-dimensional substrate for efficient hydrogen evolution. *ACS Nano* **2014**, *8*, 4940–4947. [[CrossRef](#)] [[PubMed](#)]

13. Wang, L.; Liu, X.; Luo, J.; Duan, X.; Crittenden, J.; Liu, C.; Zhang, S.; Pei, Y.; Zeng, Y.; Duan, X. Self-optimization of the active site of molybdenum disulfide by an irreversible phase transition during photocatalytic hydrogen evolution. *Angew. Chem.* **2017**, *129*, 7718–7722. [[CrossRef](#)]
14. Wang, H.T.; Lu, Z.Y.; Xu, S.C.; Kong, D.S.; Cha, J.J.; Zheng, G.Y.; Hsu, P.C.; Yan, K.; Bradshaw, D.; Prinz, F.B.; et al. Electrochemical tuning of vertically aligned MoS₂ nanofilms and its application in improving hydrogen evolution reaction. *Proc. Natl. Acad. Sci. USA* **2013**, *110*, 19701–19706. [[CrossRef](#)] [[PubMed](#)]
15. Jiao, Y.; Zheng, Y.; Jaroniec, M.; Qiao, S.Z. Design of electrocatalysts for oxygen- and hydrogen-involving energy conversion reactions. *Chem. Soc. Rev.* **2015**, *44*, 2060–2086. [[CrossRef](#)] [[PubMed](#)]
16. Zou, X.X.; Zhang, Y. Noble metal-free hydrogen evolution catalysts for water splitting. *Chem. Soc. Rev.* **2015**, *44*, 5148–5180. [[CrossRef](#)]
17. Yu, Y.F.; Huang, S.Y.; Li, Y.P.; Steinmann, S.N.; Yang, W.T.; Cao, L.Y. Layer-dependent electrocatalysis of MoS₂ for hydrogen evolution. *Nano Lett.* **2014**, *14*, 553–558. [[CrossRef](#)]
18. Zhang, J.; Hong, H.; Lian, C.; Ma, W.; Xu, X.Z.; Zhou, X.; Fu, H.X.; Liu, K.H.; Meng, S. Interlayer-state-coupling dependent ultrafast charge transfer in MoS₂/WS₂ bilayers. *Adv. Sci.* **2017**, *4*, 1700086. [[CrossRef](#)]
19. Ji, Z.H.; Hong, H.; Zhang, J.; Zhang, Q.; Huang, W.; Cao, T.; Qiao, R.X.; Liu, C.; Liang, J.; Jin, C.H.; et al. Robust stacking-independent ultrafast charge transfer in MoS₂/WS₂ bilayers. *ACS Nano* **2017**, *11*, 12020–12026. [[CrossRef](#)]
20. Murthy, A.A.; Stanev, T.K.; Dos Reis, R.; Hao, S.; Wolverson, C.; Stern, N.P.; Druavid, V.P. Direct visualization of electric-field-induced structural dynamics in monolayer transition metal dichalcogenides. *ACS Nano* **2020**, *14*, 1569–1576. [[CrossRef](#)]
21. Wu, X.; Gu, Y.; Ge, R.; Serna, M.I.; Huang, Y.; Lee, J.C.; Akinwande, D. Electron irradiation-induced defects for reliability improvement in monolayer MoS₂-based conductive-point memory devices. *NPJ 2D Mater. Appl.* **2022**, *6*, 31. [[CrossRef](#)]
22. Robinson, J.A.; Schuler, B. Engineering and probing atomic quantum defects in 2D semiconductors: A perspective. *Appl. Phys. Lett.* **2021**, *119*, 140501. [[CrossRef](#)]
23. Trainer, D.J.; Nieminen, J.; Bobba, F.; Wang, B.; Xi, X.; Bansil, A.; Iavarone, M. Visualization of defect induced in-gap states in monolayer MoS₂. *NPJ 2D Matter. Appl.* **2022**, *6*, 13. [[CrossRef](#)]
24. Huang, X.; Li, Z.; Liu, X.; Hou, J.; Kim, J.; Forrest, S.R.; Deotare, P.B. Neutralizing defect states in MoS₂ monolayers. *ACS Appl. Mater. Interfaces* **2021**, *13*, 44686–44692. [[CrossRef](#)] [[PubMed](#)]
25. Su, H.Y.; Ma, X.; Sun, K. Single-atom metal tuned sulfur vacancy for efficient H₂ activation and hydrogen evolution reaction on MoS₂ basal plane. *Appl. Surf. Sci.* **2022**, *597*, 153614. [[CrossRef](#)]
26. Cho, J.; Seok, H.; Lee, I.; Lee, J.; Kim, E.; Sung, D.; Kim, T. Activation of nitrogen species mixed with Ar and H₂S plasma for directly N-doped TMD films synthesis. *Sci. Rep.* **2022**, *12*, 10335. [[CrossRef](#)] [[PubMed](#)]
27. Liu, X.; Hou, Y.; Tang, M.; Wang, L. Atom elimination strategy for MoS₂ nanosheets to enhance photocatalytic hydrogen evolution. *Chin. Chem. Lett.* **2023**, *34*, 107489. [[CrossRef](#)]
28. Xie, L.; Wang, L.; Zhao, W.; Liu, S.; Huang, W.; Zhao, Q. WS₂ moire superlattices derived from mechanical flexibility for hydrogen evolution reaction. *Nat. Commun.* **2021**, *12*, 5070. [[CrossRef](#)]
29. Liu, M.; Li, H.; Liu, S.; Wang, L.; Xie, L.; Zhuang, Z.; Sun, C.; Wang, J.; Tang, M.; Sun, S.; et al. Tailoring activation sites of metastable distorted 1T' -phase MoS₂ by Ni doping for enhanced hydrogen evolution. *Nano Res.* **2022**, *15*, 5946–5952. [[CrossRef](#)]
30. Park, S.; Park, J.; Abroshan, H.; Zhang, L.; Kim, J.K.; Zhang, J.M.; Guo, J.H.; Siahrostami, S.; Zheng, X.L. Enhancing catalytic activity of MoS₂ basal plane S-vacancy by Co cluster addition. *ACS Energy Lett.* **2018**, *3*, 2685–2693. [[CrossRef](#)]
31. Mahler, B.; Hoepfner, V.; Liao, K.; Ozin, G.A. Colloidal synthesis of 1T-WS₂ and 2H-WS₂ nanosheets: Applications for photocatalytic hydrogen evolution. *J. Am. Chem. Soc.* **2014**, *136*, 14121–14127. [[CrossRef](#)] [[PubMed](#)]
32. Yin, Y.; Zhang, Y.M.; Gao, T.L.; Yao, T.; Zhang, X.H.; Han, J.C.; Wang, X.J.; Zhang, Z.H.; Xu, P.; Zhang, P.; et al. Synergistic phase and disorder engineering in 1T-MoSe₂ nanosheets for enhanced hydrogen-evolution reaction. *Adv. Mater.* **2017**, *29*, 1700311. [[CrossRef](#)] [[PubMed](#)]
33. Voiry, D.; Yamaguchi, H.; Li, J.W.; Silva, R.; Alves, D.C.B.; Fujita, T.; Chen, M.W.; Asefa, T.; Shenoy, V.B.; Eda, G.; et al. Enhanced catalytic activity in strained chemically exfoliated WS₂ nanosheets for hydrogen evolution. *Nat. Mater.* **2013**, *12*, 850–855. [[CrossRef](#)]
34. Tan, C.L.; Luo, Z.M.; Chaturvedi, A.; Cai, Y.Q.; Du, Y.H.; Gong, Y.; Huang, Y.; Lai, Z.C.; Zhang, X.; Zheng, L.R.; et al. Preparation of high-percentage 1T-phase transition metal dichalcogenide nanodots for electrochemical hydrogen evolution. *Adv. Mater.* **2018**, *30*, 1705509. [[CrossRef](#)] [[PubMed](#)]
35. Wang, L.; Xie, L.; Zhao, W.; Liu, S.; Zhao, Q. Oxygen-facilitated dynamic active-site generation on strained MoS₂ during photo-catalytic hydrogen evolution. *Chem. Eng. J.* **2021**, *405*, 127028. [[CrossRef](#)]
36. Guo, Y.B.; Chen, Q.; Nie, A.M.; Yang, H.; Wang, W.B.; Su, J.W.; Wang, S.Z.; Liu, Y.W.; Wang, S.; Li, H.Q.; et al. 2D hybrid superlattice-based on-chip electrocatalytic microdevice for in situ revealing enhanced catalytic activity. *ACS Nano* **2020**, *14*, 1635–1644. [[CrossRef](#)]
37. Chou, S.S.; Sai, N.; Lu, P.; Coker, E.N.; Liu, S.; Artyushkova, K.; Luk, T.S.; Kaehr, B.; Brinker, C.J. Understanding catalysis in a multiphase two-dimensional transition metal dichalcogenide. *Nat. Commun.* **2015**, *6*, 8311. [[CrossRef](#)]
38. Jin, H.Y.; Liu, X.; Chen, S.M.; Vasileff, A.; Li, L.Q.; Jiao, Y.; Song, L.; Zheng, Y.; Qiao, S.Z. Heteroatom-doped transition metal electrocatalysts for hydrogen evolution reaction. *ACS Energy Lett.* **2019**, *4*, 805–810. [[CrossRef](#)]

39. Jiao, S.; Kong, M.; Hu, Z.; Zhou, S.; Xu, X.; Liu, L. Pt atom on the wall of atomic layer deposition (ALD)-made MoS₂ nanotubes for efficient hydrogen evolution. *Small* **2022**, *18*, 2105129. [[CrossRef](#)]
40. Koudakan, P.A.; Wei, C.; Mosallanezhad, A.; Liu, B.; Fang, Y.; Hao, X.; Wang, G. Constructing reactive micro-environment in basal plane of MoS₂ for pH-universal hydrogen evolution catalysis. *Small* **2022**, *18*, 2107974. [[CrossRef](#)]
41. Wei, Z.; Tang, J.; Li, X.; Chi, Z.; Wang, Y.; Wang, Q.; Zhang, G. Wafer-scale oxygen-doped MoS₂ monolayer. *Small Methods* **2021**, *5*, 2100091. [[CrossRef](#)] [[PubMed](#)]
42. Wang, H.; Tsai, C.; Kong, D.; Chan, K.; Abild-Pedersen, F.; Nørskov, J.K.; Cui, Y. Transition-metal doped edge sites in vertically aligned MoS₂ catalysts for enhanced hydrogen evolution. *Nano Res.* **2015**, *8*, 566–575. [[CrossRef](#)]
43. Lin, W.; Zhang, B.; Jiang, J.; Liu, E.; Sha, J.; Ma, L. Anionic and cationic co-substitutions of S into vertically aligned WTe₂ nanosheets as catalysis for hydrogen evolution under alkaline conditions. *ACS Appl. Nano Mater.* **2022**, *5*, 7123–7131. [[CrossRef](#)]
44. Tayyab, M.; Hussain, A.; Syed, W.A.; Nabi, S.; Asif, Q.U.A. Effect of copper concentration and sulfur vacancies on electronic properties of MoS₂ monolayer: A computational study. *J. Mol. Model.* **2021**, *27*, 213. [[CrossRef](#)]
45. Gault, B.; Schweinar, K.; Zhang, S.; Lahn, L.; Scheu, C.; Kim, S.H.; Kasian, O. Correlating atom probe tomography with X-ray and electron spectroscopies to understand microstructure–activity relationships in electrocatalysts. *MRS Bull.* **2022**, *47*, 718–726. [[CrossRef](#)]
46. Vega-Granados, K.; Gochi-Ponce, Y.; Alonso-Vante, N. Electrochemical interfaces on chalcogenides: Some structural perspectives and synergistic effects of single-surface active sites. *Curr. Opin. Electrochem.* **2022**, *33*, 100955. [[CrossRef](#)]
47. Yin, W.; Yuan, L.; Huang, H.; Cai, Y.; Pan, J.; Sun, N.; Zhang, Q.; Shu, Q.; Gu, C.; Zhuang, Z.; et al. Strategies to accelerate bubble detachment for efficient hydrogen evolution. *Chin. Chem. Lett.* **2023**, 108351. [[CrossRef](#)]
48. Yu, H.; Zhang, M.; Cai, Y.; Zhuang, Y.; Wang, L. The Advanced Progress of MoS₂ and WS₂ for Multi-Catalytic Hydrogen Evolution Reaction Systems. *Catalysts* **2023**, *13*, 1148. [[CrossRef](#)]
49. Zhang, Y.; Pan, J.; Gong, G.; Song, R.; Yuan, Y.; Li, M.; Wang, L. In Situ Surface Reconstruction of Catalysts for Enhanced Hydrogen Evolution. *Catalysts* **2023**, *13*, 120. [[CrossRef](#)]
50. Zakerian, F.; Fathipour, M.; Faez, R.; Darvish, G. The effect of structural defects on the electron transport of MoS₂ nanoribbons based on density functional theory. *J. Theor. Appl. Phys.* **2019**, *13*, 55–62. [[CrossRef](#)]
51. Man, P.; Srolovitz, D.; Zhao, J.; Ly, T.H. Functional grain boundaries in two-dimensional transition-metal dichalcogenides. *Acc. Chem. Res.* **2021**, *54*, 4191–4202. [[CrossRef](#)]
52. Wang, G.; Wang, Y.P.; Li, S.; Yang, Q.; Li, D.; Pantelides, S.T.; Lin, J. Engineering the crack structure and fracture behavior in monolayer MoS₂ by selective creation of point defects. *Adv. Sci.* **2022**, *9*, 2200700. [[CrossRef](#)]
53. Chen, D.R.; Muthu, J.; Guo, X.Y.; Chin, H.T.; Lin, Y.C.; Haider, G.; Ting, C.; Kalbáč, M.; Hofmann, M.; Hsieh, Y.P. Edge-dominated hydrogen evolution reactions in ultra-narrow MoS₂ nanoribbon arrays. *J. Mater. Chem. A* **2023**, *11*, 15802–15810. [[CrossRef](#)]
54. Wang, S.; Li, J.; Hu, S.; Kang, H.; Zhao, S.; Xiao, R.; Sui, Y.; Chen, Z.; Peng, S.; Jin, Z.; et al. Morphology Regulation of MoS₂ Nanosheet-Based Domain Boundaries for the Hydrogen Evolution Reaction. *ACS Appl. Nano Mater.* **2022**, *5*, 2273–2279. [[CrossRef](#)]
55. Man, P.; Jiang, S.; Leung, K.H.; Lai, K.H.; Guang, Z.; Chen, H.; Huang, L.; Chen, T.; Gao, S.; Peng, Y.; et al. Salt-Induced High-Density Vacancy-Rich Two-Dimensional MoS₂ for Efficient Hydrogen Evolution. *Adv. Mater.* **2023**, 2304808. [[CrossRef](#)]
56. Zhou, Y.; Li, C.; Zhang, Y.; Wang, L.; Fan, X.; Zou, L.; Cai, Z.; Jiang, J.; Zhou, S.; Zhang, B.; et al. Controllable Thermochemical Generation of Active Defects in the Horizontal/Vertical MoS₂ for Enhanced Hydrogen Evolution. *Adv. Funct. Mater.* **2023**, 2304302. [[CrossRef](#)]
57. Mamiyev, Z.; Balayeva, N.O. Metal Sulfide Photocatalysts for Hydrogen Generation: A Review of Recent Advances. *Catalysts* **2022**, *12*, 1316. [[CrossRef](#)]
58. Mamiyev, Z.; Balayeva, N.O. PbS nanostructures: A review of recent advances. *Mater. Today Sustain.* **2023**, *21*, 100305. [[CrossRef](#)]
59. Nguyen, T.T.; Cao, T.M.; Balayeva, N.O.; Pham, V.V. Thermal treatment of polyvinyl alcohol for coupling MoS₂ and TiO₂ nanotube arrays toward enhancing photoelectrochemical water splitting performance. *Catalysts* **2021**, *11*, 857. [[CrossRef](#)]
60. Do, H.H.; Le, Q.V.; Nguyen, T.V.; Huynh, K.A.; Tekalgne, M.A.; Tran, V.A.; Kim, S.Y. Synthesis of MoS_x/Ni-metal-organic framework-74 composites as efficient electrocatalysts for hydrogen evolution reactions. *In. J. Energy Res.* **2021**, *45*, 9638–9647. [[CrossRef](#)]
61. Mosconi, D.; Till, P.; Calvillo, L.; Kosmala, T.; Garoli, D.; Debellis, D.; Granozzi, G. Effect of Ni doping on the MoS₂ structure and its hydrogen evolution activity in acid and alkaline electrolytes. *Surfaces* **2019**, *2*, 531–545. [[CrossRef](#)]
62. Pramoda, K.; Rao, C.N.R. 2D transition metal-based phospho-chalcogenides and their applications in photocatalytic and electrocatalytic hydrogen evolution reactions. *J. Mater. Chem. A* **2023**, *11*, 16933. [[CrossRef](#)]
63. Huang, Y.; Sun, Y.; Zheng, X.; Aoki, T.; Pattengale, B.; Huang, J.; Gu, J. Atomically engineering activation sites onto metallic 1T-MoS₂ catalysts for enhanced electrochemical hydrogen evolution. *Nat. Commun.* **2019**, *10*, 982. [[CrossRef](#)] [[PubMed](#)]
64. Zhao, Y.; Li, H.; Yang, R.; Xie, S.; Liu, T.; Li, P.; Zhai, T. Transient phase transition during the hydrogen evolution reaction. *Energy Environ. Sci.* **2023**. [[CrossRef](#)]

Disclaimer/Publisher's Note: The statements, opinions and data contained in all publications are solely those of the individual author(s) and contributor(s) and not of MDPI and/or the editor(s). MDPI and/or the editor(s) disclaim responsibility for any injury to people or property resulting from any ideas, methods, instructions or products referred to in the content.